Time-Reversal-Invariant Hofstadter-Hubbard Model with Ultracold Fermions

Daniel Cocks, Peter P. Orth, Stephan Rachel, Michael Buchhold, Karyn Le Hur, and Walter Hofstetter

Time-reversal invariant Hofstadter-Hubbard model with ultracold fermions

Daniel Cocks,[1, *] Peter P. Orth,[2, *] Stephan Rachel,[3] Michael Buchhold,[1] Karyn Le Hur,[4, 3] and Walter Hofstetter[1]

[1]*Institut für Theoretische Physik, Goethe-Universität, 60438 Frankfurt/Main, Germany*
[2]*Institute for Theory of Condensed Matter, Karlsruhe Institute of Technology (KIT), 76131 Karlsruhe, Germany*
[3]*Department of Physics, Yale University, New Haven, Connecticut 06520, USA*
[4]*Center for Theoretical Physics, Ecole Polytechnique, CNRS, 91128 Palaiseau Cedex, France*

We consider the time-reversal invariant Hofstadter-Hubbard model which can be realized in cold atom experiments. In these experiments, an additional staggered potential and an artificial Rashba–type spin-orbit coupling are available. Without interactions, the system exhibits various phases such as topological and normal insulator, metal as well as semi–metal phases with two or even more Dirac cones. Using a combination of real-space dynamical mean-field theory and analytical techniques, we discuss the effect of on-site interactions and determine the corresponding phase diagram. In particular, we investigate the semi–metal to antiferromagnetic insulator transition and the stability of different topological insulator phases in the presence of strong interactions. We compute spectral functions which allow us to study the edge states of the strongly correlated topological phases.

Introduction.— Ultracold quantum gases trapped in optical lattice potentials provide insight into strongly correlated condensed matter systems. Examples are the Mott-superfluid transition, the dynamics of the Hubbard model after a quench of parameters and the simulation of quantum magnetism [1]. Striking is the precise experimental control over almost all system parameters, including the particle-particle interaction strength. Simulating more traditional electronic condensed matter systems, however, is complicated by the fact that cold atoms are charge neutral, and their center of mass motion is thus not affected by external magnetic or electric fields (apart from trapping potentials). An experimental breakthrough was thus the engineering of so-called "artificial" gauge fields, which give rise to effective magnetic or electric fields for the neutral particles [2]. Remarkably, they may even be generalized to simulate spin-orbit couplings or non-Abelian fields [3]. The effective electromagnetic fields and couplings can be large, which allows, for example, to realize the quantum (spin) Hall effect in a completely new experimental context [4–8].

The underlying idea of realizing time-reversal invariant two-dimensional (2D) topological phases with cold atoms is as simple as it is fundamental [4, 8]. Consider the (integer) quantum Hall effect (QHE) on a 2D square lattice where an external magnetic field along the z–direction breaks time-reversal and translational symmetry. The single particle spectrum for arbitrary magnetic field strength – having the shape of a butterfly – was first computed by Douglas Hofstadter [9] since then referred to as the *Hofstadter butterfly*. If the magnetic flux per plaquette is a rational number $\alpha = p/q$, in units of the Dirac flux quantum $\Phi_0 = h/e$, the system remains translationally invariant with an enlarged unit cell of q lattice sites. The spectrum consists of q energy bands and in all energy gaps one finds a finite Chern number C and correspondingly $|C|$ chiral edge modes per edge. Interestingly, for even values of q the system is a semi-metal at half-filling and exhibits q Dirac cones.

To restore time-reversal symmetry we can imagine applying a magnetic field in the z–direction that only couples to the up-spins and a second field of the same strength but opposite direction that only couples to the down-spins. We thus end up with a spinful and time-reversal invariant (TRI) version of the fundamental Hofstadter problem. Remarkably, such a scenario is feasible using cold-atoms in artificial gauge fields [4, 5]. Thus, the semi-metallic Dirac dispersion for even q becomes a generalization of graphene with a tunable number of Dirac cones. Energy gaps which were crossed by a single chiral edge mode in the QHE setup are now traversed by a helical Kramer's pair of edge states, corresponding to a topological insulator phase. Note that one can use the same Gedankenexperiment to construct the Kane–Mele model [7] from two time-reversed copies of Haldane's honeycomb model [10]. The Kane–Mele model with additional Hubbard interaction has recently been intensively studied [11], in contrast to the Hofstadter problem.

In this Letter we study the effect of interactions in the (TR-invariant) *Hofstadter-Hubbard model* using real-space dynamical mean-field theory (RDMFT) [12]. We explain our numerical results using analytical arguments. We consider interaction effects on both (semi-)metallic and gapped topological phases. Although $\mathbb{Z}_2$ topological insulators are known to be robust against disorder [13, 14], rigorous and general results about the fate of topological insulators in the presence of Coulomb or Hubbard interactions are limited [15]. Some three–dimensional materials of the iridate family are possible candidates for systems where strong spin–orbit coupling and Coulomb interactions compete [16, 17]. In 2D, however, topological insulator phases have so far only been found in HgTe/CdTe quantum wells [18, 19], where Coulomb interactions seem to be negligible.

Interacting TRI Hofstadter problem.— The TRI Hofstadter-Hubbard model is described by the Hamiltonian

$$H = - \sum_j \Big\{ t_x c^\dagger_{j+\hat{x}} c_j + t_y c^\dagger_{j+\hat{y}} e^{i2\pi\alpha x\sigma^z} c_j$$
$$+ \text{h.c.} \Big\} + \sum_j U n_{j,\uparrow} n_{j,\downarrow} \,, \qquad (1)$$

where $c^\dagger_j = (c^\dagger_{j\uparrow}, c^\dagger_{j\downarrow})$ at lattice site $j = (x,y)$, σ^z is a Pauli matrix and $\hat{x} = (1,0)$, $\hat{y} = (0,1)$ are unit vectors. t_x (t_y) is the hopping amplitude in $x(y-)$ direction. We focus on isotropic hopping $t_x = t_y = t$ here, and express all energies in units of $t \equiv 1$. The value of α determines the strength of the (artificial) magnetic field for either spin species which penetrates a lattice plaquette in units of the Dirac flux quantum. The on-site interaction strength U can be experimentally tuned by Feshbach resonances and by adjusting the lattice depth. For $U = 0$ this model was studied in Ref. 4 (for experimental details see Suppl. Mat.).

We first consider the TRI Hofstadter-Hubbard problem for general $\alpha = p/q$ at half filling. For q odd the system is metallic with a nested Fermi surface, and antiferromagnetic Néel order occurs for infinitesimally small interaction $U = 0^+$ as for the ordinary square lattice. For q even the situation is very different because the system is a semi–metal (SM) at half filling [20]. The noninteracting bandstructure exhibits q Dirac cones (with a multiplicity of 2 due to spin) which are separated by momentum $2\pi/q$ in momentum space. The $\alpha = 1/2$ case is thus very similar to graphene (but note that the coordination number is $z = 4$ rather than $z = 3$). For smaller α on the other hand the system embodies a generalization of graphene with a tunable number of valleys.
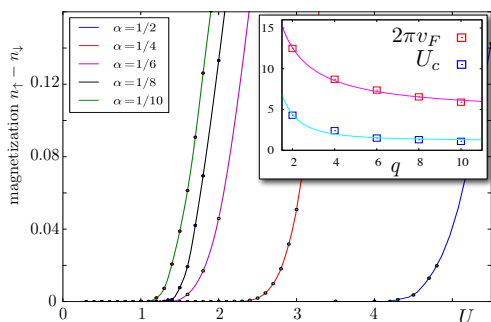
FIG. 1. (color online). Magnetization $m = n_\uparrow - n_\downarrow$ in the Néel state is plotted versus interaction strength U. We show results for $\alpha = 1/2$ (blue), $1/4$ (red), $1/6$ (magenta), $1/8$ (black), and $1/10$ (green). Inset: Fermi velocity $2\pi v_F$ (red symbols) for different $\alpha = 1/q$ is shown versus q. U_c (blue symbols) obtained within RDMFT versus q is also shown. Magenta line is a fit of v_F to $\propto 1/q$ and cyan line of U_c to $\propto 1/q^2$. Note that odd q denominators exhibit $U_c = 0^+$ due to a nested Fermi surface.

We investigate the SM–insulator transition for various $\alpha = 1/q$ (q even) within RDMFT. In Fig. 1, the magnetization is shown as a function of interaction U. The insulating phase for $U > U_c$ is antiferromagnetically (AF) ordered with a magnetization pointing in the z–direction and an ordering wave-vector $\boldsymbol{Q} = (\pi, \pi)$. We find that the critical value of U_c to enter the insulating and magnetically ordered phase decreases for increasing q. This is expected from the increased scattering that can take place between the cones. At U_c we also observe a simultaneous opening of the single particle gap. Within our approach we thus find no sign of an intermediate non-magnetic gapped phase.

To understand the behavior of $U_c(q)$ we make use of Herbut's argument [21]. Herbut considers graphene and studies the SM–insulator transition within a large-N approach, and finds that U_c depends on $2N$, the number of Dirac cones (N refers to the spin degeneracy), and the Fermi velocity v_F as $U_c \sim v_F/2N$. As shown in detail in the Supplementary Material, we are able to match our results with Herbut's analysis by replacing the Fermi velocities and $2N = qN$. In fact, from the bandstructure at $U = 0$ we find $v_F \propto 1/q$. Consequently, setting $N = 2$ for spin-1/2 particles, U_c should exhibit a $1/q^2$ behavior which agrees very well with the RDMFT data; see inset of Fig. 1. We further note that we find that $U_c(\alpha = 3/8) < U_c(\alpha = 1/8)$, which is in agreement with the analysis above since $v_F(\alpha = 3/8) < v_F(\alpha = 1/8)$.

Specific cold atom setup.— We now consider two additional terms in the Hamiltonian that are available in the cold-atom setup [4, 5]: a staggering of the optical lattice potential along the x–direction

$$H_\lambda = \sum_j (-1)^x \lambda_x c^\dagger_j c_j \,, \qquad (2)$$

and a Rashba-like spin-orbit coupling that breaks axial spin symmetry. It is introduced via replacing in Eq. (1)

$$t_x \to t_x \exp(-i2\pi\gamma\sigma^x) \,. \qquad (3)$$

We first study the effect of finite λ_x and γ on the magnetic ordering.
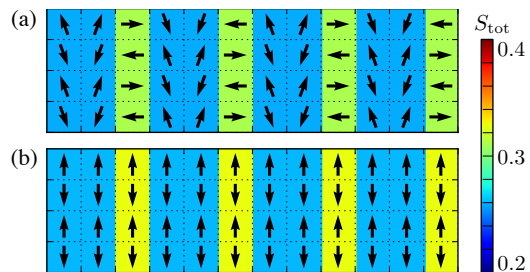
FIG. 2. (color online). Real space magnetization profile $\boldsymbol{m}(\boldsymbol{x})$ in S^y–S^z plane for $\alpha = 1/6$, $U = 5$, $\lambda_x = 0$, and $\gamma = 0.125$ (a) and $\gamma = 0.25$ (b), respectively.
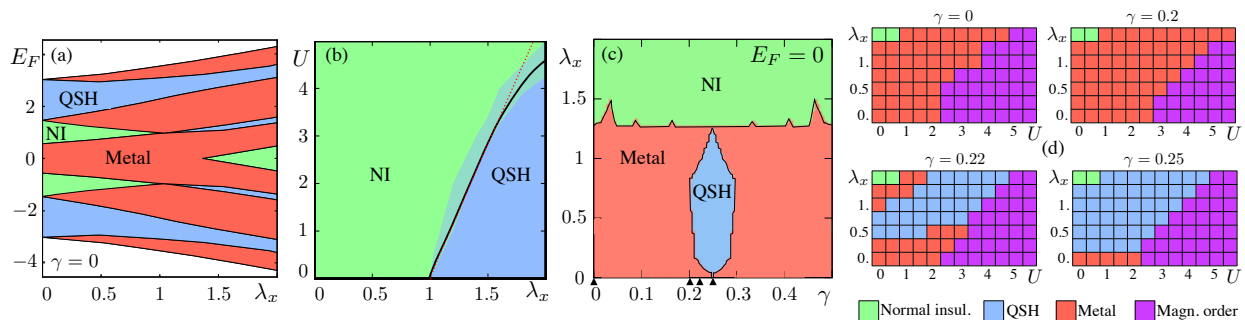
FIG. 3. (color online). (a) E_F–λ_x–phase diagram at $\gamma = U = 0$. (b) U–λ_x–phase diagram at $n_F = 2/3$ and $\gamma = 0$. (c) λ_x–γ–phase diagram at half filling $n_F = 1$ and $U = 0$. (d) U–λ_x–phase diagrams at $E_F = 0$ for various values of γ [indicated by arrows in part (a)] and inverse temperature $\beta = 20$. We find (semi–)metal (red), normal insulator (NI) (green), topological insulator (QSH) (blue), and magnetically ordered phases (purple).

Tunable magnetism.— For $\gamma = 0$, increasing λ_x increases U_c but does not change the type of magnetic order. Finite γ does, however, change the type of magnetic order in general. To demonstrate this we consider fixed $U = 5$ at $\alpha = 1/6$ and calculate the magnetization in real space for various values of $\gamma \in [0, 0.25]$. The spin operators are defined in terms of the fermionic operators as usual as $\boldsymbol{S}_j = \frac{1}{2} c_j^\dagger \boldsymbol{\sigma} c_j$ with $\boldsymbol{\sigma} = (\sigma^x, \sigma^y, \sigma^z)$. We show the magnetization pattern for $\gamma = 0.125$ and $\gamma = 0.25$ in Fig. 2 obtained within RDMFT. We obtain similar results for other values of α and γ. For $\gamma = 0.125$, the magnetization lies in the S^y–S^z plane, has a periodicity of six (two) lattice sites along $x(y)$ and reads explicitly $\boldsymbol{m}(\boldsymbol{x}) = S_{\text{tot}}(x) \cos \pi y \left(0, -\cos(\frac{\pi x}{3} + \eta), \sin(\frac{\pi x}{3} + \eta)\right)$ with $\eta = 0.39 \sin \frac{\pi x}{3} \cos \frac{\pi x}{3}$. The magnetization makes angles of $\{0°, 70°, 110°, 180°, 250°, 290°\}$ in the S^y-S^z-plane (spiral order). For $\gamma = 0.25$, the magnetic order is given by $\boldsymbol{m}(\boldsymbol{x}) = S_{\text{tot}}(x)(0, 0, \cos \pi y)$ (collinear order). Quantum fluctuations reduce the size of the magnetization $S_{\text{tot}} < 1/2$, which depends not only on the parameters α, γ and U/t, but is also spatially staggered for intermediate values of U/t (see Fig. 2). The staggering decreases for larger values of U/t. More importantly, tuning the parameter γ we pass from Néel to spiral to collinear order crossing two magnetic quantum phase transitions.

We can qualitatively understand this type of magnetic order by rigorously deriving a quantum spin Hamiltonian for even stronger interactions when charge fluctuations freeze out at half filling (see Suppl. Mat. for details)

$$\mathcal{H} = J_x \sum_j \left\{ S_j^x S_{j+\hat{\boldsymbol{x}}}^x + \cos(4\pi\gamma)\left[S_j^y S_{j+\hat{\boldsymbol{x}}}^y + S_j^z S_{j+\hat{\boldsymbol{x}}}^z \right] \right.$$

$$\left. + \sin(4\pi\gamma)\left[S_j^z S_{j+\hat{\boldsymbol{x}}}^y - S_j^y S_{j+\hat{\boldsymbol{x}}}^z \right] \right\}$$

$$+ J_y \sum_j \left\{ \cos\left(4\pi\alpha x\right)\left[S_j^x S_{j+\hat{\boldsymbol{y}}}^x + S_j^y S_{j+\hat{\boldsymbol{y}}}^y \right] + S_j^z S_{j+\hat{\boldsymbol{y}}}^z \right.$$

$$\left. + \sin(4\pi\alpha x)\left[S_j^y S_{j+\hat{\boldsymbol{y}}}^x - S_j^x S_{j+\hat{\boldsymbol{y}}}^y \right] \right\} \tag{4}$$

where $J_i = 4t_i^2/U$. The first part describes spin exchange in x–direction. For $\gamma = n/2$ with $n \in \mathbb{Z}$ we obtain a simple antiferromagnetic Heisenberg term. Other values of γ, however, break SU(2) symmetry and cause anisotropy of XXZ–type with S^x as anisotropy direction in spin space. For $\gamma \neq n/4$ there is an additional Dzyaloshinskii-Moriya (DM) interaction term in the YZ-plane, which is responsible for the spiral spin order in Fig. 2(a). Spin exchange in the y–direction is periodic with an extended unit cell in the x–direction depending on the flux $\alpha = p/q$: for odd q the unit cell contains q lattice sites, but for even q it only contains $q/2$ lattice sites, reflecting second order perturbation theory. For instance, one finds for the π–flux lattice ($\alpha = 1/2$) an ordinary Heisenberg exchange term. For other values of α the XY–term exhibits a modulation of its amplitude depending on α, while the Z–term always favors AF Ising order. The rich magnetic order predicted by the spin Hamiltonian is in agreement with our RDMFT findings.

Topological insulators.— Let us now turn to the study of interaction effects on the gapped phases. For $U = 0$, we distinguish the normal (NI) and topological (TI) insulating phases by calculating the $\mathbb{Z}_2$ invariant ν using Hatsugai's method [22]. For $U > 0$, we identify the phases by computing the spectral function in a cylindrical geometry using RDMFT and counting the number of gapless helical edge states crossing the bulk gap (for technical details we refer to the Supplementary Material). The TI phase exhibits an odd number of helical Kramer's pairs per edge while the NI phase an even number (including zero). Edge states are also crucial for detection of topological phases in cold-atom experiments, and we numerically study how robust they are with respect to interactions. In the following, we focus on fixed $\alpha = 1/6$, which qualitatively captures all phenomena that occur in this system for general $\alpha = p/q$.

In the axial symmetric case of $\gamma = 0$ there exist TI phases only away from half filling, since the system is a (semi–)metal for $n_F = 1$ (and not too large λ_x, U). This

is shown in Fig. 3(a), and is expected as the spinless Hofstadter problem at $\alpha = 1/6$ exhibits a QHE with Chern number $C = \pm 2$ for E_F in the two energy gaps closest to zero and a QHE with $C = \pm 1$ for E_F in the other gaps. The Chern number corresponds to the number of chiral edge modes in an open geometry. In the present time–reversal invariant system we thus find an according number of helical Kramer's pairs within the gaps.

For a filling of $n_F = 1/3, 5/3$ the system is thus a TI. We observe this topological phase to be stable even for large interactions up to $U = 10$. We can induce a NI–TI phase transition in the other gap for $n_F = 2/3, 4/3$ by applying a large enough staggered lattice potential $\lambda_x \geq 1$ [see Fig. 3(a)]. Fixing $n_F = 2/3$ we now turn on interactions, and observe that this phase is quite stable as shown in Fig. 3(b). Eventually, large enough interactions reverse the effect of the staggering potential and drive the system into the NI phase. Note that a static Hartree-like approximation (red dashed line) yields comparable results for small U but overestimates the effect of staggering for larger values of U.

A topological phase at half filling occurs only if we break the axial symmetry in the system by considering $\gamma > 0$. We present the non-interacting λ_x–γ phase diagram in Fig. 3(c) [4]. The interacting λ_x–U phase diagram for different values of γ, which is shown in Fig. 3(d). Both semi-metal and QSH phases are robust up to interactions of order $U \simeq 3 - 5$, at which point larger interactions drive the system into a magnetically ordered state. Prominently, we observe an interaction–driven NI to QSH transition for $\gamma = 0.25$ and $\lambda_x \gtrsim 1.5$, and a metal-QSH transition for $0.22 \leq \gamma < 0.25$ and $\lambda_x \gtrsim 1$.

Using RDMFT for a cylinder geometry, we are able to directly observe the behavior of the edge states in the interacting system. Gapless edge states are key to different detection schemes of topological phases in cold-atom systems [23, 24]. Since topological phases are uniquely characterized by their helical edge states [25], a probe of these states is the most direct measurement [4, 26]. In Fig. 4, we give an example of the spectral function $A(k_y, \omega)$ for the interaction driven NI-QSH transition at $\gamma = 0.25$, $\lambda_x = 1.5$. For $U = 0.5$, we find no gapless edge modes that are connecting the two bulk bands, corresponding to NI, while at $U = 2$ we clearly find a single pair of helical edge modes traversing the bulk gap, which corresponds to the QSH phase.

Conclusion.— We have investigated the TRI Hofstadter-Hubbard model using RDMFT complemented by analytical arguments. We quantitatively determine the interacting phase diagram including two additional terms available in the cold-atom experiment, a lattice staggering and Rashba-type spin-orbit coupling. Interactions drive various phase transitions. Similar to graphene, we find that a semi-metal at half-filling turns into a magnetic insulator at a critical finite interaction strength. Rashba-type spin-orbit interactions lead to
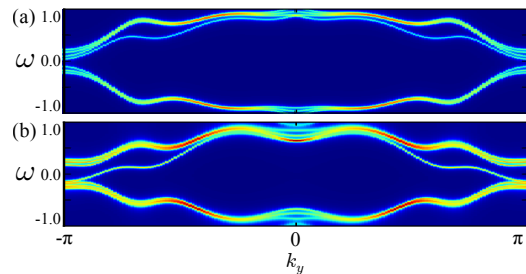
FIG. 4. (color online). Spectral function $A(k_y, \omega)$ of interacting system clearly distinguishing between (a) NI phase with no edge states traversing the bulk gap at $U = 0.5$ and (b) QSH phase at $U = 2$ with a single pair of edge modes (per edge) connecting the two bulk bands. Both plots are for $\alpha = 1/6$, $\gamma = 0.25$ and $\lambda_x = 1.5$.

tunable magnetic order with collinear and spiral phases. We explicitly demonstrate the stability of the topological phases with respect to interactions, and verify the existence of robust helical edge states in the strongly correlated TI phase, which is crucial for experimental detection schemes.

Note added.– After the submission of this work a number of other studies appeared [27] that investigate the strong-coupling limit of fermions (and bosons) in the presence of non-Abelian gauge fields using a spin Hamiltonian similar to our Eq. (4).

* These authors contributed equally to this work.
[1] W. S. Bakr *et al.*, Science **329**, 547 (2010); U. Schneider *et al.*, Nat. Phys **8**, 213 (2012); J. Simon *et al.*, Nature **472**, 307 (2011).
[2] J. Dalibard *et al.*, Rev. Mod. Phys. **83**, 1523 (2011); R. Dum and M. Olshanii, Phys. Rev. Lett. **76**, 1788 (1996); J. Ruostekoski *et al.*, Phys. Rev. Lett. **88**, 180401 (2002); D. Jaksch and P. Zoller, New J. Phys. **5**, 56 (2003); G. Juzeliunas and P. Öhberg, Phys. Rev. Lett. **93**, 033602 (2004); E. J. Mueller, Phys. Rev. A **70**, 041603(R) (2004); Y.-J. Lin *et al.*, Nature **462**, 628 (2009); M. Aidelsburger *et al.*, Phys. Rev. Lett. **107**, 255301 (2011); K. Jimenez-Garcia *et al.*, Phys. Rev. Lett. **108**, 225303 (2012); N. Cooper, Phys. Rev. Lett. **106**, 175301 (2011).
[3] A. M. Dudarev *et al.*, Phys. Rev. Lett. **92**, 153005 (2004); K. Osterloh *et al.*, Phys. Rev. Lett. **95**, 010403 (2005); J. Ruseckas *et al.*, Phys. Rev. Lett. **95**, 010404 (2005);

I. I. Satija *et al.*, Phys. Rev. Lett. **97**, 216401 (2006); N. Goldman, EPL **80**, 20001 (2007); I. I. Satija *et al.*, Phys. Rev. A **77**, 043410 (2008); Y.-J. Lin *et al.*, Nature **471**, 83 (2011); J. Struck *et al.*, Phys. Rev. Lett **108**, 225304 (2012); L. Cheuk *et al.*, Phys. Rev. Lett. **109**, 095302 (2012); P. Wang *et al.*, Phys. Rev. Lett. **109**, 095301 (2012); P. Hauke *et al.*, arXiv:1205:1398.

[4] N. Goldman *et al.*, Phys. Rev. Lett. **105**, 255302 (2010).

[5] F. Gerbier and J. Dalibard, New J. Phys. **12**, 033007 (2010).

[6] M. Z. Hasan and C. L. Kane, Rev. Mod. Phys. **82**, 3045 (2010); X.-L. Qi and S.-C. Zhang, Rev. Mod. Phys. **83**, 1057 (2011).

[7] C. L. Kane and E. J. Mele, Phys. Rev. Lett. **95**, 146802 (2005); *ibid.* **95**, 226801 (2005).

[8] B. A. Bernevig and S. C. Zhang, Phys. Rev. Lett. **96**, 106802 (2006).

[9] D. R. Hofstadter, Phys. Rev. B **14**, 2239 (1976).

[10] F. D. M. Haldane, Phys. Rev. Lett. **61**, 2015 (1988).

[11] S. Rachel and K. Le Hur, Phys. Rev. B **82**, 075106 (2010); M. Hohenadler, T. C. Lang, and F. F. Assaad, Phys. Rev. Lett. **106**, 100403 (2011); D. Soriano, J. Fernanez-Rossier, Phys. Rev. B **82**, 161302 (2010); D. Zheng, C. Wu and Z. Zhong, Phys. Rev. B **84**, 205121 (2011); S.-L. Yu, X. C. Xie, and J.-X. Li, Phys. Rev. Lett. **107**, 010401 (2011); D.-H. Lee, Phys. Rev. Lett. **107**, 166806 (2011); W. Wu, S. Rachel, W.-M. Liu, and K. Le Hur, Phys. Rev. B **85**, 205102 (2012); A. Rüegg and G. Fiete, Phys. Rev. Lett. **108**, 046401 (2012); C. Griset and C. Xu, Phys. Rev. B **85**, 045123 (2012); M. Hohenadler *et al.*, Phys. Rev. B **85**, 115132 (2012); M. Mardani, M.-S. Vaezi, and A. Vaezi, arXiv:1111.5980.

[12] A. Georges, G. Kotliar, W. Krauth, and M. J. Rozenberg, Rev. Mod. Phys. **68**, 13 (1996); M. Snoek, I. Titvinidze, C. Töke, K. Byczuk, and W. Hofstetter, New J. Phys., **10**, 093008 (2008); R. Bulla *et al.*, Rev. Mod. Phys. **80**, 395 (2008); E. Gull *et al.*, Rev. Mod. Phys. **83**, 349 (2011).

[13] J. E. Moore and L. Balents, Phys. Rev. B **75**, 121306(R) (2007).

[14] A. P. Schnyder *et al.*, Phys. Rev. B **78**, 195125 (2008); E. Prodan, T. L. Hughes, and B. A. Bernevig, Phys. Rev. Lett. **105**, 115501 (2010).

[15] C. Xu and J. E. Moore, Phys. Rev. B **73**, 045322 (2006); M. Levin and A. Stern, Phys. Rev. ett. **103**, 196803 (2009); Z. Wang, X.-L. Qi, and S.-C. Zhang, *ibid.* **105**, 256803 (2010); V. Gurarie, Phys. Rev. B **83**, 085426 (2011); J. C. Budich *et al.*, arXiv:1203.2928.

[16] D. A. Pesin and L. Balents, Nature Phys. **6**, 376 (2010).

[17] M. Kargarian, J. Wen, and G. A. Fiete, Phys. Rev. B **83**, 165112 (2011).

[18] B. A. Bernevig, T. L. Hughes, and S.-C. Zhang, Science **314**, 1757 (2006).

[19] M. König *et al.*, Science **318**, 766 (2007).

[20] M. Kohmoto, Phys. Rev. B **39**, 11943 (1989).

[21] I. F. Herbut, Phys. Rev. Lett. **97**, 146401 (2006).

[22] T. Fukui and Y. Hatsugai, Phys. Rev. B **75**, 121403 (2007).

[23] T. D. Stanescu *et al.*, Phys. Rev. A **79**, 053639 (2009); T. D. Stanescu *et al.*, *ibid* **82**, 013608 (2010); H. M. Price and N. R. Cooper, *ibid* **85**, 033620 (2012); X.-J. Liu *et al.*, *ibid* **81**, 033622 (2010); B. Béri and N. R. Cooper, Phys. Rev. Lett **107**, 145301 (2011).

[24] R. O. Umucalilar *et al.*, Phys. Rev. Lett. **100**, 070402 (2008); E. Zaho *et al.*, Phys. Rev. A **84**, 063629 (2011); E. Alba *et al.*, Phys. Rev. Lett. **107**, 235301 (2011).

[25] C. Wu, B. A. Bernevig, and S.-C. Zhang, Phys. Rev. Lett. **96**, 106401 (2006);

[26] N. Goldman, J. Beugnon, and F. Gerbier, Phys. Rev. Lett. **108** 255303 (2012). M. Buchhold, D. Cocks, and W. Hofstetter, Phys. Rev. A **85**, 063614 (2012).

[27] M. Gong *et al.*, arXiv:1205.6211; W. S. Cole *et al.*, Phys. Rev. Lett. **109**, 085302 (2012); J. Radic *et al.*, Phys. Rev. Lett. **109**, 085303 (2012); Z. Cai *et al.*, Phys. Rev. A **85**, 061605(R) (2012).